9th European Workshop on Structural Health Monitoring
July 10-13, 2018, Manchester, United Kingdom

A case study in quantifying the economic benefit of a live strain monitoring campaign for a short-span pre-stressed concrete bridge

Piotr Omenzetter[1], Pilate Moyo[2] and James M. W. Brownjohn[3]
1) The Lloyd's Register Foundation Centre for Safety and Reliability Engineering, The University of Aberdeen, Scotland
2) The University of Cape Town, South Africa
3) The University of Exeter, UK

Abstract

A short-span pre-stressed concrete bridge was the subject of several in-situ experimental investigations and analyses including experimental modal analyses and continuous live strain monitoring campaigns. Data from the latter was used to examine whether the cost of carrying the monitoring exercise can be justified by a tangible reduction in the risk of structural failure as assessed with the benefit of the data. To that end, the bridge risk was quantified initially using structural reliability methods and loads mandated by a design code but without any information from monitoring, and then the risk assessment was repeated with the measured strain data incorporated into the process. The comparison of the two risk values enabled quantifying the value of information derived from structural health monitoring, which was found to bring an overall net benefit.

1 Introduction

The Pioneer Bridge (Figures 1 and 2) is located in Singapore across a storm drain on a busy road serving the Jurong Port. The bridge was built between 1968 and 1970 and was sized for the then-prevailing design loads and following the design philosophy of the era [1]. Originally, it comprised 37 pre-cast pre-tensioned inverted T-beams spaced by 0.507 m centre-to-centre, clearly visible in Figure 2, tied together by 25 cast in-situ 203 mm thick transverse diaphragms set at a 762 mm centre-centre spacing. The simply-supported span length was 18.16 m between elastomeric bearings, and the total width was 18.796 m with four lanes of width of 3.82 m each available to traffic. The T-beams carried a deck slab having thickness varying from 152 mm to 305 mm. At the turn of the millennium, deemed unfit for the forecast future increased traffic volumes and axle loads the structure was strengthened as part of the wider Singapore's Land Transport Authority's (LTA) program of highway bridge upgrading. This transformed the simple supported span into an integral bridge with continuity between the T-beams and slab and the abutments provided by a densely reinforced monolithic connection.

The refurbishing works and LTA's willingness to offer the bridge as a testbed, provided researchers from Nanyang Technological University, where the three co-authors of this paper worked or studied at the time, the perfect opportunity to develop and evaluate in-situ a portfolio of experimentally based bridge structural condition and performance assessment techniques. These past investigations are documented primarily in Brownjohn et al. [2] and Moyo et al. [3], with ancillary insights provided e.g. in [4], and comprised:

- Two one-off in-situ experimental model analyses and modal system identifications in the pre- and post-upgrade stage,
- Finite element model updating exercises using the experimental modal data to assess quantitatively the structural changes brought about by strengthening,
- Two approximately month-long continuous live strain monitoring campaigns under real traffic conditions in the pre- and post-upgrade stage, and
- Statistical analyses of the recorded live strains to assess improvement in load bearing capacity due to upgrading.

The current paper focuses on the results of pre-upgrading strain monitoring exercise and re-examines these historical data to evaluate, a posteriori, the economic benefit of undertaking the

monitoring campaign. The motivation is that while various benefits of structural health monitoring (SHM) are often strongly asserted, these claims are still rarely backed up by quantitative cost-benefit analysis even though the cost of SHM deployment may, and not infrequently is, relatively high. We demonstrate how information derived from SHM data can be used to update quantitative risk assessment outcome and in doing so justify and rationalise the expenditure on SHM.

In the paper, firstly the pre-upgrading strain monitoring campaign is briefly overviewed. This is followed by quantitative risk assessments of bridge failure, initially without SHM information using loads derived solely from a design code, and subsequently utilizing live load effects (strains) measured in-situ under real operational conditions. The risk assessment is based on the classical structural reliability approaches and estimation of cost/consequences of failure.

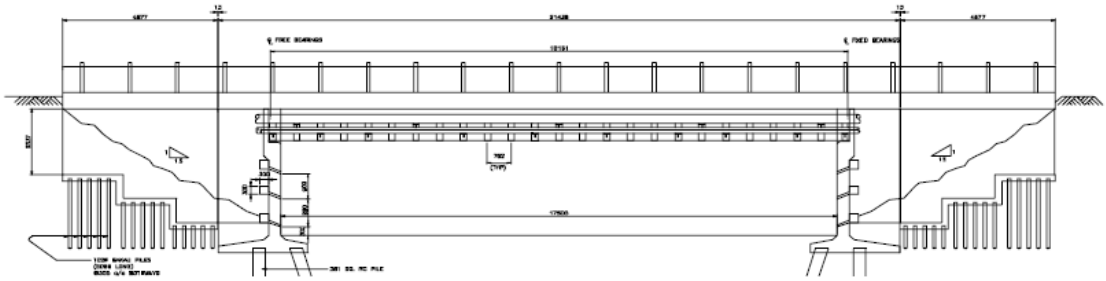

Figure 1 – Side view of Pioneer bridge before upgrading.

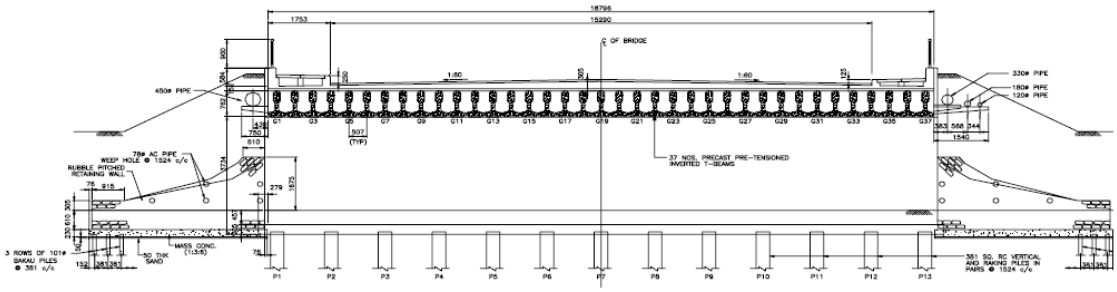

Figure 2 – Cross-sectional view of Pioneer bridge before upgrading.

2 Pre-upgrading live strain monitoring campaign

The live strain monitoring program [3] involved measurement of dynamic strains at the bridge mid-span using a purpose-made bridge monitoring system. The monitoring system comprised four demountable strain gauges (Figure 3), and a data acquisition box with sampling rate up to 500 Hz. The data acquisition system was powered by a 12 V battery, enabling use in remote sites such as the Pioneer bridge. Recording was triggered by ambient traffic at a selected level of strain. For each above-threshold event the strain waveform, peak values, and date and time were stored. The strain gauges were mounted on the soffits of girders 7, 15, 24, 33 (see Figure 2), i.e. approximately under the centre of each of the four traffic lanes 1-4. The pre- and post-upgrading SHM campaigns lasted at least 20 days.

Most of the recorded peak live strains were concentrated between 6.00 am and 00.00 midnight and evenly distributed over that period. The results clearly showed that most of heavy vehicles used lane 1 and lane 2, while lane 4 experienced little heavy traffic during the monitoring period. However, the maximum live strain recorded prior to upgrading works was 172 με and occured on lane 3.

Figure 3 – Demountable strain gauge attached to bridge soffit.

3 Quantitative bridge failure risk assessment

This section is devoted to demonstration of a practical application of SHM-assisted quantitative risk assessment and comprises, firstly, an assessment of the Pioneer bridge pre-upgrading reliability based on prior (i.e. pre-monitoring) information available about the structure and design loads prescribed in codes, and, secondly, updating of the reliability assessment using live strains recorded on the bridge. An estimation of cost and consequences of bridge failure follows enabling quantification of failure risk and discussing the economic benefits of the in-situ SHM campaign.

3.1 Pre-monitoring structural reliability assessment

In the absence of any monitoring information, a bridge would be evaluated in the lead up to its potential upgrading or replacement using any available historical information such as as-designed and/or as-built drawings, specifications and documents, visual inspection reports, material testing results, etc. Loads as specified by the relevant codes and standards would be assumed if site-specific data were unavailable, which is normally the case in practice. A similar approach is taken in this section for pre-monitoring assessment of the Pioneer bridge.

However, assessing later the value of SHM information entails estimating probability of failure. Thus, reliability-based assessment needs to be undertaken requiring formulation of limit state functions and probabilistic models for demands (loads) and structural resistance. This contrast with the pragmatic, but rather simplistic, ways uncertainties are handled via partial safety factors in most of contemporary design codes. In this context, however, the UK code BD21/01 [5], which is used in Singapore, states that 'it was shown that the ultimate load (i.e. 1.5×HA) occurred with a return period of 200,000 years'. This gives the return period for exceedance of T=200,000 years and the annual probability of exceedance $p=1/T=5\times10^{-6}$. Fitting a Gumbel (i.e. double exponential) extreme value distribution [6], whose generic form of the cumulative distribution function for a random variable x is [7]:

$$F(x)=\exp\left(-\exp\left(-(x-\lambda)/\alpha\right)\right) \tag{1}$$

requires calibration of the location parameter, λ, and the scale parameter, α. The information on annual exceedance probability alone is not sufficient and so the scale parameter was assumed to be the same as estimated from measured traffic strains [3] used in the subsequent section. The location parameter can then be calculated by inverting the Gumbel cumulative distribution function:

$$\lambda = x - \alpha \ln\left(-\ln\left(1-p\right)\right) \tag{2}$$

where x is the value of code-prescribed HA load.

The HA load in BD21/01 [5] comprises concurrent uniformly distributed load (UDL), and knife edge load (KEL) acting over traffic lanes in the way that produces maximum demand. The detailed recipes how to arrive at the numerical values of the UDL and KEL for a structure at hand depend on span length, traffic lane widths and numbers, heavy traffic volumes and quality of surface. For the span length of 18.16 m, traffic lane width of 3.82 m (>3.56 m), reduction factor K=0.835 assumed as the average of those given for the range of heavy traffic volumes and surface conditions given in BD21/01 [5], and spacing between T-beams of 0.507 m, the values of UDL and KEL were found as 58.72 kN/m and 20.32 kN, respectively, for a single T-beam. Note, two interwoven assumptions were made, namely, that all four traffic lanes are equally loaded to the maximum HA load (i.e. all lane factors equal one) and that no load redistribution occurs, i.e. each beam takes on all the loads acting directly over it. This will result in a conservative assessment but is not believed to introduce significant error nonetheless as the in-situ strain monitoring campaign [3] and theoretical work [4] both concluded that load redistribution between T-beams was weak. The parameters of the Gumbel distributions of live loads are summarised in Table 1.

The remining loads that were considered comprised dead loads from self-weight of the T-beams, from average slab thickness and diaphragms distributed uniformly over the entire bridge deck, and from asphalt. For these calculations, concrete specific weight was taken as 24 kN/m^3, that of asphalt as 23 kN/m^3, structural dimensions from drawings were used and asphalt thickness was assumed as 50 mm. Normal distributions were adopted with coefficients of variation (COVs) suggested by Nowak [8]. The parameters of all statistical distributions of dead loads are summarised in Table 2.

Table 1 – Parameters of live load Gumbel distributions

Load	Symbol	BD21/01 value	Location parameter, λ	Scale parameter, α
UDL	p_{UDL}	58.72 kN/m	-207.96 kN/m	21.85 kN/m
KEL	P_{KEL}	20.32 kN	-246.36 kN	21.85 kN

Table 2 – Parameters of dead load normal distributions

Load	Symbol	Mean, μ	COV
T-beams	q_T	6.23 kN/m	8%
Slab and diaphragms	q_s	5.63 kN/m	10%
Asphalt	q_a	0.58 kN/m	25%

Table 3 – Parameters of T-beam resistance normal distributions

Parameter	Symbol	Mean, μ	COV
'Section strength'	EZ	2.15 MNm	10%
Strain to first yield	$\Delta\varepsilon_y$	1240 με	10%

The only limit state function adopted considers flexural failure at the mid-span of the simply-supported T-beams due to tensional failure (onset of first yield) of pre-stressing strands. For uniformity with the SHM data considered later, the limit state function and failure criterion for a vector random variable $\mathbf{x}$=[EZ $\Delta\varepsilon_y$ q_T q_s q_a p_{UDL} P_{KEL}]' is expressed in terms of the strain in strands as:

$$G(\mathbf{x}) = \Delta\varepsilon_y - \frac{(q_T + q_s + q_a)L^2/8 + p_{UDL}\,L^2/8 + P_{KEL}\,L/4}{EZ} < 0 \tag{3}$$

where L is the span length, E is T-beam concrete Young's modulus (calculated from in-situ concrete core samples as 34.9 GPa), Z is the section modulus calculated at the level of the lowest strands, and $\Delta\varepsilon_y$ is the remaining strain before the first yield of strands after pre-stressing strain, including any rheological losses, has been subtracted. The other symbols in Equation (3) were introduced and explained in Tables 1 and 2.

In calculating the mean value of section modulus, a fully composite action between the T-beams and the slab was assumed, the latter having Young's modulus of 80.5% of the T-beams (from in-situ material samples), leading to the 2nd moment of inertia of 1.27×10^{-3} m^4 [2]. The pre-stressing strands were assumed to have a diameter of 10 mm and concrete cover of 30 mm, resulting in Z=6.17×10^{-2} m^3. The combined 'section strength' parameter EZ was assigned a normal distribution with the mean value of 2.15 MNm, and a COV of 10%, respectively. Following Moyo et al. [3], a stress-strain curve from BD 44/95 [9] was adopted for the strands that indicates the first yield at 5000 με, and 30% rheological pre-stressing losses were assumed, leaving 1240 με to be utilized for servicing the dead and live loads. This value was taken as the mean, together with the COV of 10% to model $\Delta\varepsilon_y$ as a normal distribution. Table 3 summaries the statistical modelling of bridge T-beam resistance to bending failure.

A first order reliability method (FORM) algorithm [7] was used for calculating the failure probability. To simplify calculations, the limit state function was reformulated slightly by bringing the EZ factor to the numerator as

$$G(\mathbf{z}) = EZ\Delta\varepsilon_y - (q_T + q_s + q_a)L^2/8 + p_{UDL}\,L^2/8 + P_{KEL}\,L/4 < 0 \tag{4}$$

Replacing all the stochastic variables x_i (i=EZ, $\Delta\varepsilon_y$, T, s, a, UDL, KEL) in the limit state function with standard normal variables z_i=$(x_i$-$\mu_i)/\sigma_i$, collated in vector $\mathbf{z}$, leads to

$$\begin{aligned}\bar{G}(\mathbf{z}) = {} & (\mu_{EZ} + \sigma_{EZ} z_{EZ})\left(\mu_{\Delta\varepsilon_y} + \sigma_{\Delta\varepsilon_y} z_{\Delta\varepsilon_y}\right) - (\mu_T + \sigma_T z_T + \mu_s + \sigma_s z_s + \mu_a + \sigma_a z_a)L^2/8 \\ & + \left(\lambda_{UDL} - \alpha_{UDL}\ln\left(-\ln\Phi(z_{UDL})\right)\right)L^2/8 + \left(\lambda_{KEL} - \alpha_{KEL}\ln\left(-\ln\Phi(z_{KEL})\right)\right)L/4 < 0\end{aligned} \tag{5}$$

where $\Phi(z)$ is the standard normal cumulative distribution function, and μ_i and σ_i are the means and standard deviations, respectively. The Rackwitz-Fiessler FORM algorithm [7] adopted herein is based on iterative application of the following equation to find the 'design point' $\mathbf{z}^*$, being the point on the limit state hyper-surface closest to the origin of the coordinate system $\mathbf{z}$:

$$z_i^{*(j+1)} = \frac{\partial\bar{G}\left(\mathbf{z}^{*(j)}\right)}{\partial z_i} \times \frac{\sum_{i=1}^{N}\frac{\partial\bar{G}\left(\mathbf{z}^{*(j)}\right)}{\partial z_i} z_i^{(j)} - \bar{G}\left(\mathbf{z}^{*(j)}\right)}{\sum_{i=1}^{N}\left(\frac{\partial\bar{G}\left(\mathbf{z}^{*(j)}\right)}{\partial z_i}\right)^2} \tag{6}$$

The iteration step is indicated by superscript (j).

Once convergence is achieved, the safety index, β, can be found as the Euclidian norm of the design point vector:

$$\beta = \left\|\mathbf{z}^*\right\| \tag{7}$$

and (approximate) failure probability as

$$P_f \approx \Phi(-\beta) \tag{8}$$

The iterative calculations, terminated at j=4 due to rapid convergence, are shown in Table 4. The resulting annual probability of failure of a single T-beam is $P_{f,1beam,1year}=\Phi(-4.5910)=2.2\times10^{-6}$. Over the period of 50 years of service this gives overall probability of failure of $P_{f,1beam,50years}=1-(1-P_{f,1beam,1year})^{50}=1.1\times10^{-4}$. Taking a single T-beam failure as sufficient to declare the whole bridge as failed and assuming the 37 T-beams will fail independently of one another, the bridge failure over the service life of 50 years will occur with a probability of $P_{f,bridge,50years}=1-(1-P_{f,1beam,50years})^{37}=4.06\times10^{-3}$.

Table 4 – FORM iterations for pre-monitoring assessment

Iteration	0	1	2	3	4
z_T	0	0.0341	0.0206	0.0219	0.0219
z_s	0	0.0382	0.0231	0.0245	0.0245
z_a	0	0.0102	0.0062	0.0066	0.0066
z_{UDL}	3	4.8934	4.5846	4.5725	4.5725
z_{KEL}	0	0.1888	0.1223	0.1265	0.1270
z_{EZ}	0	-0.4416	-0.2556	-0.2760	-0.2761
$z_{\Delta\varepsilon_y}$	0	-0.4416	-0.2556	-0.2760	-0.2761
$\partial\bar{G}(\mathbf{z})/\partial z_T$	-20.6116	-20.6116	-20.6116	-20.6116	-20.6116
$\partial\bar{G}(\mathbf{z})/\partial z_s$	-23.0850	-23.0850	-23.0850	-23.0850	-23.0850
$\partial\bar{G}(\mathbf{z})/\partial z_a$	-6.1835	-6.1835	-6.1835	-6.1835	-6.1835
$\partial\bar{G}(\mathbf{z})/\partial z_{UDL}$	-2958.9433	-4578.4583	-4310.2308	-4299.8097	-4299.7778
$\partial\bar{G}(\mathbf{z})/\partial z_{KEL}$	-114.1794	-122.1451	-119.2579	-119.4379	-119.4592
$\partial\bar{G}(\mathbf{z})/\partial z_{EZ}$	267.0129	255.2222	260.1891	259.6427	259.6405
$\partial\bar{G}(\mathbf{z})/\partial z_{\Delta\varepsilon_y}$	267.0129	255.2222	260.1891	259.6437	259.64045
$\bar{G}(\mathbf{z})$	5861.5232	-1517.7920	-40.6212	-0.0519	0.0000
β	3.0000	4.9370	4.6005	4.5910	4.5910

3.2 SHM-data based assessment

Strains obtained in the pre-upgrading continuous monitoring campaign [3] were analysed here using a similar approach to the one of the previous Section 3.1. The structural and dead load models were unchanged, but the live loads were replaced with their directly measured effects (strains). Moyo et al. [3] report Gumbel distributions for daily maximum strains recorded on the Pioneer bridge over a period of approximately one month. These were resampled using a Monte Carlo approach [7] to obtain annual maxima and new Gumbel distributions were fitted to the resampled data. The reason for proceeding in that way was two-fold: i) to align the assessment time interval with the previous section, and ii) to avoid computational issues resulting from extremely low, practically zero, probabilities of daily exceedance of structural resistance. The Gumbel distribution of maximum annual strains, ε_L, from the most strained of the four monitored T-beams (designated as girder 24 under traffic lane 3 in [3]) are shown in Table 5.

Table 5 – Statistical properties of measured live load strains

Life load effect	Symbol	Location parameter, λ_L	Scale parameter, α_L
Strain	ε_L	143.63 kN/m	21.85 kN/m

The corresponding limit state function is

$$\bar{G}_{SHM}\left(\mathbf{z}_{SHM}\right)=\left(\mu_{EZ}+\sigma_{EZ}z_{EZ}\right)\left(\mu_{\Delta\varepsilon_y}+\sigma_{\Delta\varepsilon_y}z_{\Delta\varepsilon_y}\right)-\left(\mu_T+\sigma_T z_T+\mu_s+\sigma_s z_s+\mu_a+\sigma_a z_a\right)L^2/8 \\ +\left(\lambda_L-\alpha_L\ln\left(-\ln\Phi\left(z_L\right)\right)\right)<0 \tag{9}$$

where the final term comprises the location and scale parameters of the measured live load strains listed in Table 5, and z_L is the standard normal variable for these. The FORM algorithm iterations are shown in Table 6. The resulting annual probability of failure of a single T-beam is in this case $P_{f,1beam,1year}=\Phi(-6.9049)$ and is extremely low, i.e. of the order of 10^{-12}. Over 50 years of service life, the order of failure probability of a T-beam is only 10^{-10}, and of the entire bridge it is 10^{-9}. For all practical reasons, this is nil and will be taken as such in our subsequent analyses.

Table 6 – FORM iterations for post-monitoring assessment

Iteration	0	1	2	3	4
z_T	0	0.2889	0.5804	0.6920	0.6951
z_s	0	0.3235	0.6501	0.7751	0.7785
z_a	0	0.0867	0.1741	0.2076	0.2085
z_L	3	1.0060	1.0266	1.2335	1.3393
z_{EZ}	0	-3.7423	-4.7052	-4.7467	-4.7303
$z_{\Delta\varepsilon_y}$	0	-3.7423	-4.7052	-4.7467	-4.7303
$\partial\bar{G}(\mathbf{z})/\partial z_T$	-20.6116	-20.6116	-20.6116	-20.6116	-20.6116
$\partial\bar{G}(\mathbf{z})/\partial z_s$	-23.0850	-23.0850	-23.0850	-23.0850	-23.0850
$\partial\bar{G}(\mathbf{z})/\partial z_a$	-6.1835	-6.1835	-6.1835	-6.1835	-6.1835
$\partial\bar{G}(\mathbf{z})/\partial z_L$	-71.7786	-36.4556	-36.7395	-39.7149	-41.3183
$\partial\bar{G}(\mathbf{z})/\partial z_{EZ}$	267.0129	167.0881	141.3790	140.2690	140.7075
$\partial\bar{G}(\mathbf{z})/\partial z_{\Delta\varepsilon_y}$	267.0129	167.0881	141.3790	140.2690	140.7075
$\bar{G}(\mathbf{z})$	1869.3298	336.5958	24.7508	-0.2580	-0.0771
β	3.0000	5.4053	6.7912	6.9070	6.9049

3.3 Cost, consequences and quantitative risk assessment

The multifaceted, complex and inherently uncertainty-laden topic of bridge failure consequences has been treated comprehensively by Imam and Chryssanthopoulos [10]. They categorized failure consequences into four main groups: human, economic, environmental and social. Examples of the most important consequences in each category are shown in Table 7. Recently, Limongelli et al. [11] used that guideline inside the hypothetical example of a bridge failing in an earthquake to assess the associated costs. The following assessment for the Pioneer bridge draws on [11] while adjusting accordingly the monetary values adopted. This preliminary evaluation is rather a guestimate showing the way towards future more precise consequence

quantification than being detailed, accurate or complete. Only selected human, economic and environmental costs are considered, as indicted by asterisks in Table 7, as the societal consequences are more elusive to put financial value on.

The human consequences considered are related to fatalities and injuries. When the bridge fails vehicles already present on it at that time, or advancing towards, may fall or collide with one another. The probability of those events occurring is a function of the expected number of vehicles passing over or approaching the bridge and depends on the typical vehicle counts and speed. Assuming average daily traffic of 10,000 vehicles (i.e. a vehicle every 8.4 sec on average), with a 70%/30% car/truck mix, an average vehicle speed of 50 km/h and a stopping distance of 25 m, gives approximately 0.36 vehicles affected. Further, assuming 2 persons per vehicle and that 10% of them will die, whereas 50% will sustain injuries with long-term consequences, and combining these assumptions with the average cost of life of €3M and that of long-term consequence injuries of €3M [12], results in the overall human cost of €1.29M.

The total cost of a short span bridge replacement in the USA, inclusive of materials, labour, equipment and engineering, was estimated by Barker [13] at $\$120/ft^2$. This translates for the Pioneer bridge to €360K. Assuming it will take two months (60 days) to fully restore the road network functionality and a detour of a length of 6 km ensuring similar traffic throughput will need be utilised during that time, the indirect economic costs can be assessed as follows. The additional indirect economical costs are related to increased fuel consumption and loss of time while navigating the detour. The fuel consumption can be taken as 0.05 l/km for the average car and 0.35 l/km for the average truck, respectively, whereas the average fuels cost as €1.50/l. Over the assumed 60 days of disruption, the total cost of additional fuel burnt will thus be €7.56M. The total cost of time lost, taking a €30/h/person unit cost [14], is €4.32M. For quantifying the environmental cost of additional CO_2 and NO_x emissions, the average emissions of 1 kg/km for CO_2 and 4.5 g/km for NO_x [15] and their costs of €0.057/kg and €34.7/kg, respectively, were used, yielding a total cost of €0.77M.

Taken together the overall cost of €6.73M multiplied by the pre-monitoring failure probability, the risk is $4.06\times10^{-3}\times$€6.73=€27.3K. This contrasts with the negligible risk concluded from the analysis of monitoring data and so represents up to how much the pre-upgrade monitoring campaign could have saved in term of better informed risk assessment. To calculate the actual savings, SHM own cost would have to be subtracted. It is not expected it exceed €27.3K, and so it is rather evident that a net benefit could easily be achieved.

Table 7 - Consequences of bridge failure (adopted from [10])

Category	Example
Human	Deaths* Injuries* Psychological trauma
Economic	Repair or replacement costs* Loss of functionality/downtime* Traffic delay/re-routing/management costs* Clean up costs Rescue costs Regional economic losses Loss of production/business/opportunity Investigations/compensations Loss of other infrastructure services (e.g. electricity, communication cables carried by the bridge)
Environmental	CO_2/NO_x emissions* Energy use Pollutant releases Environmental clean-up/reversibility
Social	Reputational damage Diminished public confidence in infrastructure Undue changes in professional practice

*) Indicates categories considered Pioneer bridge risk evaluation.

4 Conclusions

This paper used a short-span concrete bridge as a case study to assess quantitatively the economic benefit of carrying out an in-situ life stain monitoring camping. To evaluate the value of information extracted from SHM data, the bridge failure risk was calculated twice: initially following the structural reliability principles and using loads prescribed by a design code but without the benefit of SHM data, and subsequently with the measured strain data fully integrated into the risk quantification process. This enabled updating the risk of failure of the structure and led to a conclusion that the cost of carrying the HSM camping was well justified.

Future research will refine the results obtained so far by attempting to model failure consequences more accurately and employing more sophisticated structural models. The value of other testing exercises, such as experimental modal analysis, and actions, such as bridge refurbishment, will also be assessed using the available experimental results.

Acknowledgements

Piotr Omenzetter works within the Lloyd's Register Foundation Centre for Safety and Reliability Engineering at the University of Aberdeen. The foundation helps to protect life and property by supporting engineering-related education, public engagement and the application of research. COST Action TU1402 Quantifying the Value of Structural Health Monitoring is acknowledged for providing the intellectual momentum and Pan-European collaborative opportunities sustaining this research effort.

References

[1] United Kingdom Ministry of Transport (1961). Standard highway loadings, Memo No. 771, Her Majesty's Stationery Office, London, UK.

[2] Brownjohn, J.M.W., Moyo, P., Omenzetter, P., Lu, Y. (2003). Assessment of highway bridge upgrading by dynamic testing and finite element model updating. *Journal of Bridge Engineering*, *ASCE*, **8**(3), pp. 162-172.

[3] Moyo, P., Brownjohn, J.M.W., Omenzetter, P. (2003). Highway bridge live loading assessment and load carrying capacity estimation using a health monitoring system. *Structural Engineering and Mechanics*, **18**(5), pp. 609-626.

[4] Omenzetter, P., Moyo, P., Brownjohn, J.M.W., Tan, B.L. (2002). Conditional assessment of highway bridge by dynamic testing and model updating. *Proc. International Conference on Structural Dynamics Modeling: Test, Analysis, Correlation and Validation*, Madeira, pp. 645-654.

[5] The Highways Agency (2001). *BD21/01: The assessment of highway bridges and structures*. The Highways Agency.

[6] Das, P.C. (2001). Assessment loading criteria for bridge decks, piers and parapets. *Structures and Buildings*, *ICE*, **146**(4), pp. 411-421.

[7] Melchers, R.E. (1999). *Structural reliability analysis and prediction*. Wiley.

[8] Nowak, A.S. (1993). Live load model for highway bridges. *Structural Safety*, **13**, pp. 53-66.

[9] The Highways Agency (2008). BD 44/95: The assessment of concrete highway bridges and structures. The Stationary Office, London, UK.

[10] Imam, B.M., Chryssanthopoulos, M.K. (2012) Causes and consequences of metallic bridge failures. *Structural Engineering International*, **22**(1), pp. 93-98.

[11] Limongelli, M.P., Miraglia, S., Fathi, A. (2018). The value of visual inspection for the emergency management of bridges under seismic hazard. *6th International Symposium on Life-Cycle Civil Engineering*, IALCEE, Ghent, 8 pp.

[12] Daniell, J.E., Schaefer, A.M., Wenzel, F., Kunz-Plapp, T. (2015). The value of life in earthquakes and other natural disasters: historical costs and the benefits of investing in life safety. *Proc. 10th Pacific Conference on Earthquake Engineering*, Sydney, 11 pp.

[13] Barker, M. (2017). Bridge economy and life cycle costs of steel and concrete bridges. NACE 2017 Short Span Steel Bridge Workshop Cincinnati, OH http://www.countyengineers.org/assets/Presentations/2017/sun%20sssb%20econ%20barker.pdf, accessed 06/05/2018.

[14] Department for Transport (2017). *Transport analysis guidance (TAG) data book*. Department for Transport UK.

[15] Muncrief, R. (2016). *NO_X emissions from heavy-duty and light-duty diesel vehicles in the EU: comparison of real-world performance and current type-approval requirements*. ICCT International Council on Clean Transportation.